Aerospace Science and Technology 71 (2017) 30–41

Contents lists available at ScienceDirect

Aerospace Science and Technology

www.elsevier.com/locate/aescte

Comprehensive preliminary sizing/resizing method for a fixed wing – VTOL electric UAV

Maxim Tyan [a], Nhu Van Nguyen [b], Sangho Kim [a], Jae-Woo Lee [a,*]

[a] Department of Aerospace Information Engineering, Konkuk University, Seoul, Republic of Korea
[b] Viettel Aerospace Institute, Viettel Group, Hanoi, Viet Nam

ARTICLE INFO

Article history:
Received 13 January 2017
Received in revised form 27 March 2017
Accepted 7 September 2017
Available online 12 September 2017

Keywords:
Electric propulsion
Aircraft design
Integrated analysis
UAV
VTOL
Sizing/resizing

ABSTRACT

A Fixed Wing (FW) aircraft with Vertical Takeoff and Landing (VTOL) is a new type of aircraft that inherits the hovering, VTOL, and maneuvering properties of multicopters and the power-efficient cruising of an FW aircraft. This paper presents a comprehensive method for FW-VTOL electric UAV sizing and resizing. The method uses newly developed integrated analysis that combines the VTOL propulsion sizing method with modified FW aircraft sizing theories. Performance requirements are specified as a set of functional relations. Several new empirical equations are derived using available data. The required battery capacity and total mass are determined from mission analysis that includes both VTOL and FW mission segments. The design is iteratively resized when the actual components of the propulsion system are selected. A case study of a 3.5-kg FW-VTOL electric UAV is presented in this research. The results of sizing and resizing are compared to parameters of the actual aircraft manufactured. Prediction of most parameters stays within a 10% error threshold.

1. Introduction

Interest in electric propulsion in different areas of transportation has grown drastically during the past decade. Mass production of electric cars, bicycles, and other transportation systems has forced the development of electric aircraft technologies. Small and medium-sized electric unmanned aerial vehicles (UAVs) are available on the market; however, their endurance is still about five times less than that of similar sized aircraft powered by internal combustion engines (ICEs) [1]. Today, electric powered vehicles mostly use lithium-ion type batteries. Current technology makes it possible to obtain an energy density of 100–200 Wh/kg and 250–400 Wh/l [2], while an ICE with kerosene fuel provides roughly 1600 Wh/kg [3]. Li-Ion batteries technology rapidly approaches the theoretical capacity limit of 370 Wh/kg [4]. Energy density of 350–380 Wh/kg with has been achieved in long endurance UAV "Zephyr" with Li–S battery [5]. Luongo et al. forecast that the emerging lithium–sulfur and lithium–oxygen technologies will provide energy densities of up to 1250 and 1750 Wh/kg in the year 2025 with theoretical limits of 2570 and 3500 Wh/kg for Li–S and Li–O_2 batteries respectively [6]. Hepperle makes a similar forecast [3]. It is expected that Li-Ion, Zn–air, Li–S, and Li–O_2 batteries will have 250, 400–500, 500–1250, and 800–1750 Wh/kg energy density respectively by year of 2025 with theoretical limits of 390, 1090, 2570, and 3500 Wh/kg. Another component of electric propulsion is the motor. While the development of electric motors for large commercial aircraft is still a big issue [3], lightweight motors under 250 kW are already available [7]. Following the technological trends, small and medium-sized electric aircraft will be able to compete with conventional ICE-powered aircraft in the near future.

Multicopter-type UAV systems have become extremely popular in recent years. Multicopters have a number of advantages compared to other types of aircraft. The multicopter structure does not contain complex mechanical parts like a helicopter swashplate. It is assembled from a chassis, control board, direct drive motors, and propellers. Simple control is performed by changing the voltage of the motor, which affects the propeller rotation speed (RPM) [8]. Lightweight control boards (autopilots), electric motors, batteries, and other components are commercially available. Multicopters are widely used due to their high maneuverability, ease of control, and vertical takeoff and landing (VTOL) capabilities. The main disadvantage of multicopters is their high power consumption, which results in relatively short operational time, typically less than half an hour. On the other hand, fixed wing (FW) aircraft provide greater power efficiency for the cruising flight, resulting in longer endurance and/or higher payload capability. The development of multicopter systems leads to the development of a new

* Corresponding author.
E-mail address: jwlee@konkuk.ac.kr (J.-W. Lee).

http://dx.doi.org/10.1016/j.ast.2017.09.008
1270-9638/

Nomenclature

AR	Wing aspect ratio		
b	Wing span	m	
b_{HT}	Horizontal tail span	m	
b_{VT}	Vertical tail span	m	
C_D	Drag coefficient		
C_L	Lift coefficient		
$C_{L_{max}}$	Maximum lift coefficient		
c_{prop}	Propeller clearance	m	
C_{HT}	Horizontal tail volume coefficient		
C_{VT}	Vertical tail volume coefficient		
D_{prop}	Propeller diameter		
DL	Disc loading	N/m^2	
e	Oswald efficiency factor		
E_{spec}	Specific energy capacity	Wh/kg	
η_p	Propeller efficiency		
h	Flight altitude		
M	Mass	kg	
MF	Mass fraction		
P	Motor power	W	
q	Dynamic pressure		
R	Flight range	m	
R/C	Rate of climb	m/s	
ρ	Air density	kg/m^3	
S_w	Wing area	sq. m	
S_{HT}	Horizontal tail area	m^2	
S_{VT}	Vertical tail area	m^2	
S_p	Propeller disc area	m^2	
S_{tot}	Total projected area of an aircraft	m^2	
t	Flight endurance	s	
T	Thrust	N	
U	Battery voltage	V	
V	Aircraft velocity	m/s	
W	Weight	N	
x_{CG}	Location of aircraft CG	m	
x_{PF}	Front propeller location	m	
x_{PR}	Rear propeller location	m	
x_{VT}	Location of vertical tail leading edge	m	

Subscripts

batt	Battery
mot	Motor
req	Required
TO	Takeoff

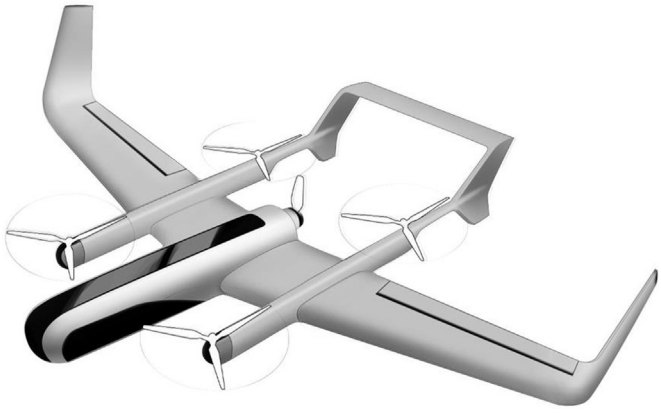

Fig. 1. FW-VTOL UAV concept.

type of VTOL aircraft that has a conventional FW configuration with an additional multicopter style VTOL propulsion system. Fig. 1 shows the concept of an FW-VTOL UAV. This configuration inherits the advantages of both schemes. It is able to replace UAV systems that are currently used for aerial mapping and surveillance and to enter the developing market of personal delivery aircraft. Table 1 summarizes the features of all three aircraft schemes.

The current UAV market for aerial mapping and surveillance is represented by small hand-launched FW UAVs (Precision Hawk Lancaster, senseFly eBee, and similar systems) and medium-sized catapult-launched UAVs (UAV Factory Penguin BE and similar), which have certain limitations in terms of payload mass and portability.

Methods of estimating the size, mass, and power of aircraft intended to meet performance and mission requirements are of great importance for aircraft design. There are several well-known sizing methodologies for FW aircraft [7–12].

Raymer has introduced the initial weight estimation method based on mission profile and a set of empirical equations [9]. The method is valid for a wide range of ICE-powered aircraft. However, there is no option to consider for electric and multicopter type propulsion systems. Significant effort was addressed to the sizing of electric FW UAVs by Gundlach [13]. The methodology presents an efficient way of calculating the battery mass fraction required for FW cruising flight as well as suggestions for UAV mass breakdown. Riboldi and Gualdoni have proposed an integrated approach for the sizing of manned electric FW aircraft [14]. Keith and Hall [15] have proposed a sizing methodology for heavy ICE-powered VTOL aircraft with MTOW of up to 27.5 tonnes. Currently the selection of a multicopter propeller and motor is performed based on simple suggestions of gear manufacturers and the designer's own experience. This research presents a novel methodology for sizing of FW-VTOL electric UAVs. The new methodology combines existing knowledge about fixed and rotary wing aircraft with newly derived statistical relations and an integrated approach. Mission and performance requirements are converted into an initial guess of future aircraft mass, geometry, and propulsion system pa-

Table 1
Comparison of multicopters, fixed wing and FW-VTOL aircraft schemes.

	Multicopter	Fixed wing aircraft	FW-VTOL aircraft
Takeoff/landing	VTOL	Runway, catapult	VTOL/STOL
Hovering	Yes	No	Yes
Maneuvering	Very agile	Medium	Medium
Stability	Unstable	Stable in forward flight	Stable in forward flight
Range, endurance	Low	High	Medium
Forward speed	Low	High	High
Payload	Low	High	Medium
Control system	Propeller RPM change	Control surface deflection	Both

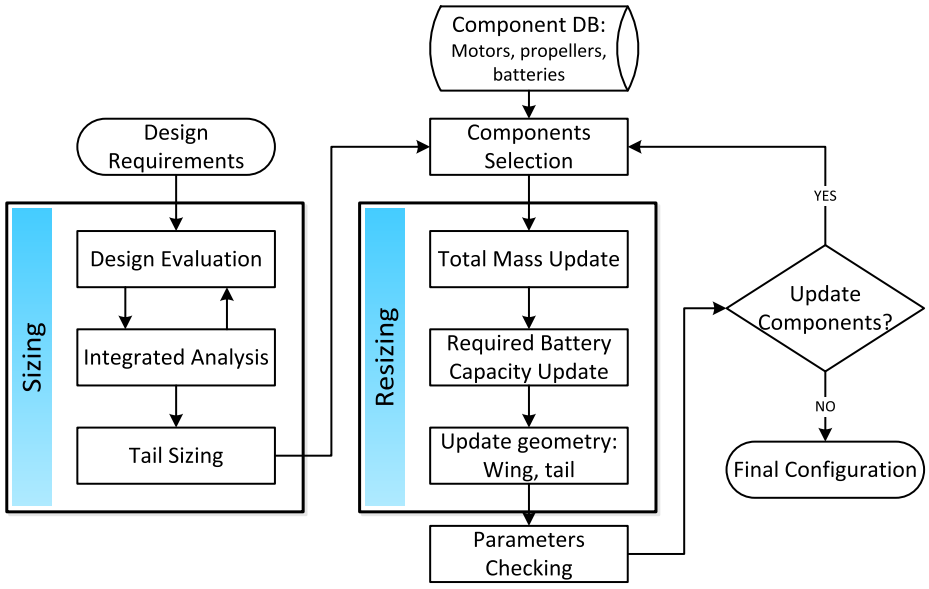

Fig. 2. FW-VTOL electric UAV preliminary sizing/resizing process.

rameters. The initial design is then resized to consider the actual components of the aircraft.

The case study is presented to demonstrate the developed approach to preliminary sizing/resizing of a FW-VTOL electric UAV. A 3.5 kg aircraft is designed using the proposed methodology. The small UAV is a part of larger 25 kg UAV development project. The main objectives of a 3.5 kg FW-VTOL electric UAV are evaluation of efficiency of FW-VTOL configuration, validation of selected sizing/resizing approach, and testing control algorithms.

2. Preliminary sizing/resizing process

The objectives of the sizing process are to determine the major parameters of mass, geometry, and propulsion of a future aircraft based on a set of design requirements and to refine them using the information about the exact components of the propulsion system and battery. Fig. 2 shows the process of sizing an FW-VTOL electric UAV.

The overall process starts from creating the set of performance and mission requirements. Initial sizing is performed next using the "rubber propulsion" model. It is assumed that there is a motor, propeller, and battery, which perfectly match the calculated parameters (power available, mass, efficiency). The initial geometry, mass, and required parameters of the propulsion system are calculated at this stage. The actual models of electric motors, propellers, and batteries should be selected after the basic parameters of propulsion are calculated. The total mass of the aircraft is updated based on new mass data of motors, propellers, and batteries. The capacity of the battery required to accomplish the mission profile is determined based on the updated mass of the aircraft, power of the motors, propeller diameter, and specific capacity of the battery. Wing and tail geometry of the aircraft are then recalculated using new total mass value. Required motor power and propeller diameter depend on total mass of an aircraft as discussed in the next section. Previously selected components are compared to new required values at parameters checking stage. If the difference between selected component's parameter (e.g. motor power) and newly calculated requirement is large then new component should be selected from the products available on a market. The process is repeated if the difference between mass and power estimated at the initial sizing stage and the resized values is large.

The key component of the process is the initial sizing. It is based on integrated analysis, which includes analytical and statistical methods in order to access the basic aircraft characteristics, and design evaluation, which estimates the best possible combination of design parameters in order to achieve the required level of performance. There are two options for design evaluation. Numerical optimization minimizes the selected metric (for example the total mass) subject to a set of design constraints. Sizing matrix plots allow the designer to visualize the contours of the target functions and to select the best design or designs for future development. Fig. 3 shows the dataflow of the initial sizing process.

The integrated analysis part is divided into three major stages: constraints analysis, propulsion analysis, and mass analysis. The wing loading (W/S) and power loading (P/W) are the design variables required to evaluate the basic characteristics of an aircraft. The feasibility of the combination of design variables in FW mode is evaluated at the constraints analysis stage. Propulsion and mass analysis is composed of several coupled analysis modules. The thrust-to-weight ratio required to maintain the given rate-of-climb and hover in VTOL motion is evaluated first. The inputs for VTOL propulsion sizing are wing loading provided by design evaluation module and total mass that comes from fixed-point iteration. The required power of the electric motor and the diameter of propellers are calculated next. The propulsion mass calculation module estimates the total mass of electric propulsion for both FW and VTOL propulsion systems. The required battery capacity and its mass fraction are calculated at the mission analysis stage. Calculated and assumed values of the components' masses are then summed to estimate the total mass (M_{TO}) of an aircraft. The calculated M_{TO} is then used as a feedback to the analysis modules. This feedback is resolved using a fixed-point iteration strategy. The solution typically converges within three to five iterations. Many of the aircraft parameters here are defined as mass or weight ratios (e.g. wing loading, thrust to weight ratio, mass fractions, etc.). Total mass is essential parameter to evaluate the actual parameters of an aircraft.

2.1. Integrated analysis

This section describes the details of the analysis methods used for initial sizing. The parabolic drag model is assumed to represent aircraft aerodynamics. Total aircraft drag has the form:

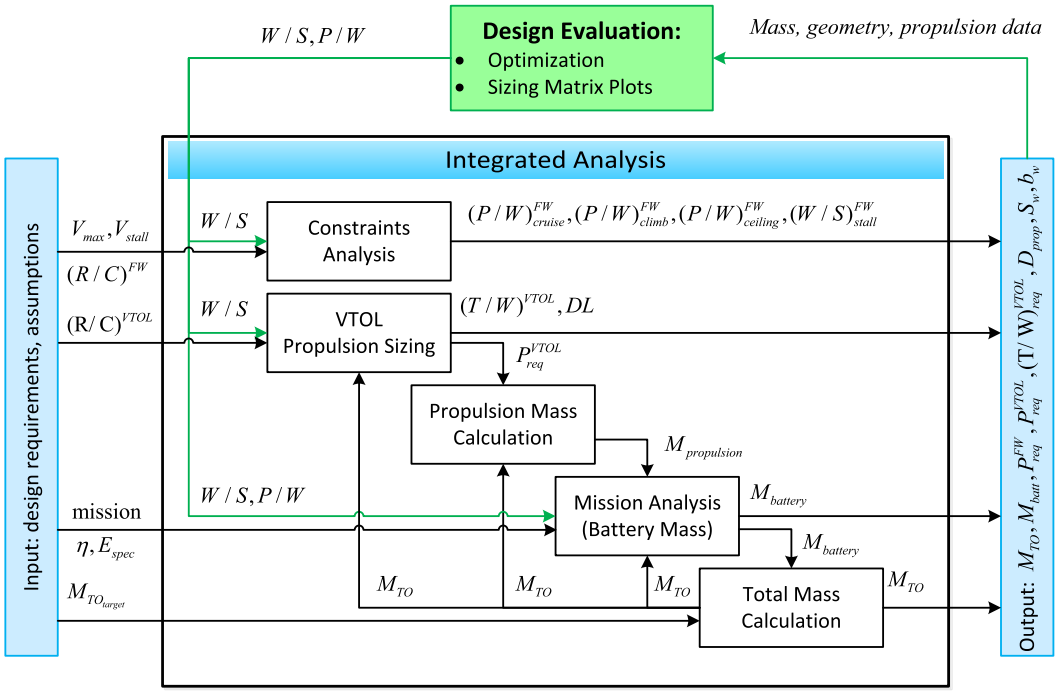

Fig. 3. FW-VTOL electric UAV sizing process.

$$C_D = C_{D_0} + kC_L^2 \tag{1}$$

$$k = \frac{1}{\pi e AR} \tag{2}$$

C_{D_0} is the minimum drag coefficient. Gudmundsson suggests the use of the value of 0.028 to 0.035 for a typical fixed gear general aviation aircraft [10]. An FW-VTOL UAV has additional tail booms for VTOL propulsion and propellers, and thus a higher value of parasite drag should be used. The recommended value of C_{D_0} for this type of aircraft is 0.035–0.040. Often the minimum drag of cambered airfoils occurs at non-zero lift coefficient and adjusted drag model equation should be used. However, use of simplified uncambered wing model is common for early conceptual design stages [13]. Raymer states that uncambered drag polar is valid for aircraft with moderate camber [9]. Adjusted drag polar can be used at preliminary design stages when more information about selected airfoil, and overall aircraft configuration is available. e is the Oswald's span efficiency factor. Gundlach [13] suggests the use of values of 0.65–0.72 for initial sizing purposes.

2.1.1. Constraints analysis

Constraint analysis is used to evaluate the feasibility of the performance constraints and to visualize the relations between two key parameters of an aircraft: wing loading and power loading. The general format of the constraint analysis graph is a two-dimensional design space such that the x-axis represents the wing loading and the y-axis the power loading. Constraints analysis requires some performance characteristics to be described in the form $P/W = f(W/S)$. In some cases it is easier to derive equations in the form $T/W = f(W/S)$. In that case, the conversion can be carried out as [10]:

$$P/W = \frac{(T/W)V}{\eta_p} \tag{3}$$

where V is the aircraft velocity and η_p is the propeller efficiency in a current flight state. Unlike piston engines, electric motors are independent of air density, and thus power normalization to sea level conditions is not needed. Battery capacity correction due to low temperature may be required in some special cases. The equation below is used to calculate the T/W ratio required to fly at a given cruise speed and altitude [10].

$$(T/W)^{FW}_{cruise} = q \cdot C_{D_0} \frac{1}{W/S} + k\frac{1}{q} W/S \tag{4}$$

$$q = \frac{1}{2}\rho V^2 \tag{5}$$

Here q is the dynamic pressure at a given airspeed and altitude. The $(T/W)^{FW}_{cruise}$ ratio for the maximum rate of climb in a fixed wing mode is calculated as follows [10]:

$$(T/W)^{FW}_{climb} = \frac{R/C}{V_{RoC}} + \frac{q}{W/S} C_{D_0} + \frac{k}{q}(W/S) \tag{6}$$

where the velocity for the best rate of climb is:

$$V_{RoC} = \sqrt{\frac{2}{\rho} W/S \sqrt{\frac{k}{3C_{D_0}}}} \tag{7}$$

This equation can also be used for calculating the service ceiling constraint. The service ceiling is the altitude where the maximum rate of climb is 100 ft/min (0.5 m/s). An FW-VTOL UAV is typically designed to fly at relatively low altitude. Typical application for this class of UAVs is a small package delivery, area monitoring, precision agriculture, and similar missions. Delivery within small range does not require cruising at high altitudes. Flight at safe altitude of less than 150 m is possible. Precision agriculture requires soil mapping with image resolution up to 2 cm/pixel [16]. This resolution can be obtained when flying at altitudes from 50 to 500 m depending on selected sensor [17]. The air density at 500 m altitude is only 5% less than at sea level. The service ceiling parameter is not critical and may be skipped in case of low altitude operations. The upper bound for the aircraft's wing loading is determined by a stall speed requirement in an FW mode. The wing loading required to maintain the stall speed is calculated as:

$$(W/S)^{FW}_{stall} = \frac{1}{2} V^2_{stall} \rho C_{L_{max}} \tag{8}$$

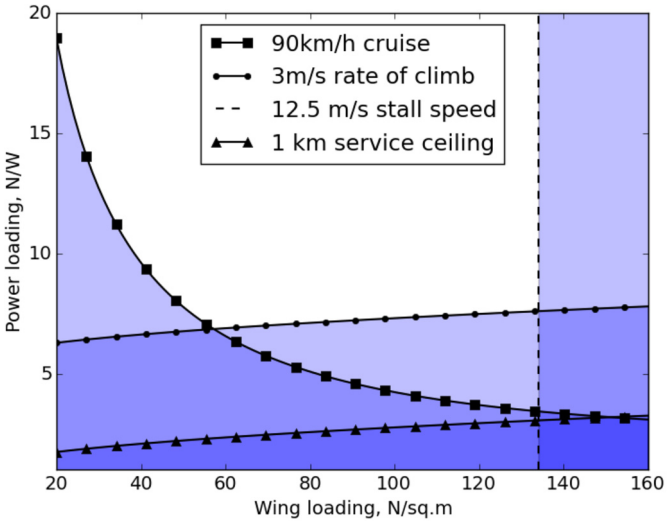

Fig. 4. Example of constraints diagram.

This type of aircraft theoretically does not stall. However, it is important to estimate the stall speed to design the transition phase from hovering to FW forward flight. The stall speed constraint also limits the minimum size of the wing. In case a FW aircraft starts to stall in forward flight, recovery in FW style is the most efficient. The aircraft should lower its nose to increase the speed. Recover using VTOL propulsion is also possible. It may consume more power and control efforts. In this case the aircraft should be slowed down at high thrust of VTOL propulsion, then rotated and finally hover. Fig. 4 shows an example of a constraints diagram for some arbitrary performance requirements. In this example, the feasible design space is the area above the cruise speed curve at low wing loading, above the rate of climb curve at high wing loading, and to the left hand side of the stall speed curve. Infeasible area is filled with color. Any solution placed inside the feasible region satisfies the performance requirements.

The constraint analysis module is connected to the design evaluation module directly without providing data to other analysis modules.

2.1.2. Total mass calculation

The total mass of an aircraft is the sum of all its components. For some components, it is possible to calculate mass; for others, mass fractions. The component mass fraction MF is the ratio of the component mass to the aircraft takeoff mass. The takeoff mass of an aircraft is the sum of the empty, payload, and energy source masses [13].

$$M_{TO} = M_{empty} + M_{payload} + M_{energy} \tag{9}$$

The energy source of an electric aircraft is a battery. Expanding the empty mass to represent the aircraft systems will give the equation below:

$$M_{TO} = M_{struct.} + M_{subsyst.} + M_{avion.} + \left(M^{VTOL}_{propulsion} + M^{FW}_{propulsion}\right) + M_{payload} + M_{battery} \tag{10}$$

Here the mass of the payload is the only value explicitly provided by the design requirements. Assumptions should be made for the structure, subsystem, and avionics mass fractions since there is still not enough data for this type of aircraft to construct the statistical models. Gundlach proposes the values of 25–35% for structure mass fraction of a FW UAV [13]. In this research, initial assumption for FW-VTOL UAV is 30–40% to account for additional structural elements to support VTOL propulsion. The avionics mass fraction of 5% is used based on the same reference. Mass fraction of subsystem may vary depending on aircraft. Aircraft designed for delivery is typically equipped with small camera for real time monitoring and delivery package mounts, thus subsystem mass fraction may be assumed 5–7%. Aircraft with advanced surveillance equipment may have subsystem mass fraction up to 15%. The total mass equation is then modified as:

$$M_{TO} = \frac{M^{VTOL}_{propulsion} + M^{FW}_{propulsion} + M_{payload}}{1 - (MF_{batt} + MF_{struct} + MF_{subsyst} + MF_{avion})} \tag{11}$$

Fig. 3 shows that the propulsion and battery mass calculation requires M_{TO} as an input. This recursion is resolved using fixed-point iteration. The initially assumed value of M_{TO} is iteratively refined until the change becomes negligibly small.

Table 2
Area ratio of different aircraft models.

Aircraft model	Type	S_{proj}/S	S_w
UAV Factory Penguin B	FW	1.41	0.79
TAM 5	FW	1.29	0.71
Precision Hawk Lancaster 3	FW	1.39	0.33
Autec Robotics Kestrel	FW-VTOL	1.24	0.82
Arcturus Jump-15	FW-VTOL	1.39	N/A
Arcturus Jump-20	FW-VTOL	1.30	2.62
Aerosonde HQ	FW-VTOL	1.46	N/A

2.1.3. VTOL propulsion sizing

An FW-VTOL UAV uses a multicopter type propulsion system for vertical takeoff, landing, axial climb, descent, and transition to forward flight. The force equilibrium equation in vertical flight can be written as follows:

$$T = W + D \tag{12}$$

The aircraft projection plane is perpendicular to the climb velocity vector. For this configuration of an aircraft, the flat plate drag assumption is valid. The flat plate drag coefficient is:

$$C_D = 2\sin^3\alpha \tag{13}$$

Then C_D is equal to 2.0 in vertical motion ($\alpha = 90°$). The force equilibrium equation can then be written in the form:

$$T^{VTOL}_{climb} = W + \frac{1}{2}\rho(R/C)^2_{VTOL}S_{proj}C_D = W + \rho(R/C)^2_{VTOL}S_{proj} \tag{14}$$

The tail and fuselage produce a large portion of the drag in vertical motion and thus cannot be neglected. The parameter S_{proj}/S is introduced to account for those contributors. This parameter describes the ratio of total projected aircraft area to wing area. This ratio can be measured from initial sketches or existing aircraft drawings of similar configuration. Area ratio of seven existing aircraft models is measured to determine the average value of the parameter. Table 2 shows the measured aircraft data.

As an initial guess, S_{proj}/S can be assumed to be 1.3–1.4. Substituting the new parameter into the equation and performing some manipulations, the final equation for calculating the required thrust-to-weight ratio in vertical climbing motion is as follows:

$$(T/W)^{VTOL}_{climb} = 1.2\left(1 + \frac{1}{W/S}\rho(R/C)^2(S_{tot}/S_w)\right) \tag{15}$$

Here, 20% more thrust is needed for trim and for withstanding wind gusts. The thrust-to-weight ratio can also be selected based on experience. Table 3 shows the recommended values of throttle setting for hovering and the corresponding T/W for multicopter design. In this research, the maximum of two values is used.

Table 3
Recommended values of thrust-to-weight ratio [18].

	Hover throttle setting	T/W
Camera platforms	70%	1.43
Aerial photography	60%	1.67
First person view (FPV) aerial explorer	50%	2.00
FPV race copters	45%	2.22

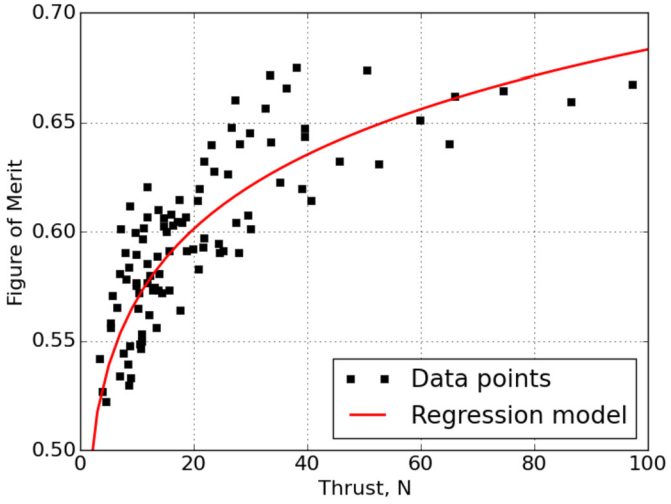

Fig. 5. Figure of merit as a function of propeller thrust.

Propeller momentum theory uses the following equation for calculating the power required to generate the required thrust [19]:

$$P_{req}^{VTOL} = \frac{T v_i}{FM} \tag{16}$$

Here, v_i is the air-induced velocity through the rotor disc, and FM is the rotor efficiency, also known as the Figure of Merit. FM varies between 0.7 and 0.8 for large helicopter rotors [19]. Multicopter propellers have a simple geometry and lower aspect ratio compared to helicopter rotor blades. The efficiency of multicopter rotors is lower. Experimental data for 85 motor–propeller combinations [20] have been processed to construct the statistical model of the FM as a function of multicopter propeller thrust.

Fig. 5 shows the experimental data points and constructed regression model to represent the FM at the initial sizing stage. The data set contains samples with FM from 52 to 67% measured at thrust from 3 to 97 N. The experimental data has a scattered behavior, thus the regression model fit with $R^2 = 0.36$. The regression model is then:

$$FM = 0.4742 \cdot T^{0.0793} \tag{17}$$

Axial climb is essential for determining the required power of the motor. From momentum theory, the induced velocity for axial climb is calculated as follows:

$$\frac{v_i}{v_h} = -\frac{(R/C)^{VTOL}}{2v_h} + \sqrt{\left(\frac{(R/C)^{VTOL}}{2v_h}\right)^2 + 1} \tag{18}$$

Here, v_h is the induced velocity in hover.

$$v_h = \sqrt{\frac{T}{2\rho S_p}} \tag{19}$$

T is the thrust generated by a single propeller at a given flight state. To calculate the VTOL propeller diameter, a database of several commercially available models of multicopters has been constructed to set up a statistical regression model. The database is constructed from 11 multicopters with different numbers of propellers and total masses from 2 to 18 kg.

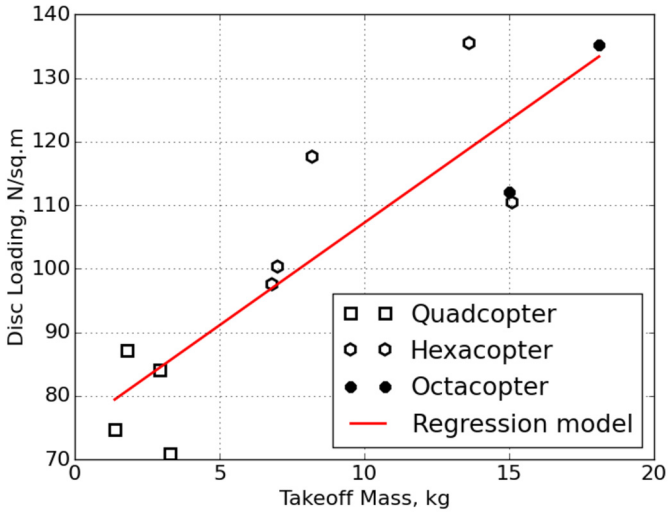

Fig. 6. Multicopter disc loading versus takeoff mass data points.

Table 4
Motor weight parameters [13].

Motor class	F_1	E_1	E_2
Brushless ferrite	7.765	−0.632	0.596
Brushed rare earth	8.160	−0.961	1.166
Brushless inrunner	13.17	−0.610	0.067
Brushless outrunner	0.889	−0.288	0.1588

Multicopter disc loading (DL) as a function of total mass is constructed with $R^2 = 0.77$. Fig. 6 shows the data points and linear curve fit. The disc loading and propeller area can then be calculated as follows:

$$DL = 3.2261 M_{TO} + 74.991 \tag{20}$$

$$S_{prop} = \frac{W_{TO}}{DL \cdot n_{prop}} \tag{21}$$

S_{prop} is the propeller disc area.

2.1.4. Electric propulsion mass calculation

The mass of the electric motor can be calculated in terms of the weight-to-power ratio. Empirical equation by Gundlach is used for prediction of motor and controller mass [13].

$$\frac{W_{mot}}{P_{max}} = F_1 P_{max}^{E_1} U_{max}^{E_2} \tag{22}$$

Table 4 shows the empirical coefficients for different classes of motors. Brushless outrunner motors are the most widely used type of electric motor in electric aircraft. The mass fraction is also highly dependent on the maximum voltage. There are a number of standard battery cell voltages available on the market: 7.2, 7.4, 8.4, and 11.1 V. Battery cells are usually combined for higher capacity and voltage. Composite cells produce a voltage equal to the sum of different cells, and thus battery cells with 14.8, 22.2, and 44.4 V are available for medium sized electric UAVs. The mass of the electric speed controller (ESC) is also determined from the following empirical equation [13]:

$$M_{ESC} = F_{ESC} P_{max}^{E_1} \tag{23}$$

Here, the coefficients F_{ESC} and E_1 have values of 0.7383×10^{-4} and 0.8854 respectively. The method described by Roskam [21] is

used for calculation of the propeller mass. The equation converted to the SI unit system is shown below.

$$M_{prop} = 6.514 \times 10^{-3} K_{material} K_{prop} n_{props} n_{blades}^{0.391} \left(\frac{D_{prop} P_{max}}{1000 n_{prop}} \right)^{0.782} \quad (24)$$

Here, an K_{prop} value of 15 is recommended for propellers with engine power of less than 50 HP. N_{props} is the number of propellers, n_{blades} the number of blades, D_{prop} the propeller diameter, and P_{max} the maximum power of all motors. The correction factor $K_{material}$ was added to the original equation to account for different materials of a propeller. A value of 1.3 can be used for wooden propellers, while 1.0 is used for plastic and 0.6 for composite. The total mass of the electric propulsion system is then determined as the sum of the electric motor, controller, and installation effects.

$$M_{propulsion} = f_{install} \left(n_{mot} \left((W_{mot}/P_{max}) \frac{P_{mot}}{g} + M_{ESC} \right) + M_{prop} \right) \quad (25)$$

The propeller diameter for FW propulsion is calculated using Raymer's method [9]:

$$D_{prop} = K_p \sqrt[4]{P_{mot}} \quad (26)$$

K_p is equal to 0.1072, 0.0995, 0.0938 for two-, three-, and four-blade propellers.

2.1.5. Battery mass calculation

The mass of the battery depends on the mission profile defined in the design requirements, the specific energy of the battery, and the total mass of the aircraft. The mass of the battery is directly proportional to its energy and inversely proportional to the specific energy, battery efficiency, and usable capacity. The general equation for the battery mass fraction is then:

$$MF_{battery} = \frac{tP}{M_{TO} E_{spec} \eta_{batt} f_{usable}} \quad (27)$$

Here t is the duration of a given mission segment and P is the power required. The power required to hover is defined in Eq. (16). Substituting it into Eq. (27) and performing some manipulations will give us the equation for the mass fraction required to hover for a certain amount of time.

$$MF_{batt}^{hover} = \frac{t_{hover} g}{E_{spec} FM \eta_{electric} \eta_{batt} f_{usable}} \sqrt{\frac{DL}{2\rho}} \quad (28)$$

Thus, the lower the disc loading, the longer the time for which multicopter and FW-VTOL aircraft are able to hover. The main limitation in using a lower disc loading is the large propeller diameter. Heavy multicopters typically have a high disc loading, as shown in Fig. 6. The power required in axial climb can be determined as shown in the VTOL propulsion sizing subsection. The time in climb and descent is determined as:

$$t_{climb} = \frac{h_{end} - h_{start}}{(R/C)_{VTOL}} \quad (29)$$

The axial descent equation is only valid for $(R/C)^{VTOL}/v_h \leq -2$; otherwise hovering during $t_{descent}$ is assumed. An aircraft may cover the maximum range in a flight condition when the ratio of velocity to power required is maximized. The battery mass fraction for this flight state is calculated as:

$$MF_{batt} = \frac{Rg}{E_{spec} \eta_{electric} \eta_{batt} f_{usable} (L/D)_{max}} \quad (30)$$

The second case is the maximum endurance flight. This occurs in the condition when the power required is minimized.

$$MF_{batt} = \frac{t_{loiter} g}{E_{spec} \eta_{electric} \eta_{batt} f_{usable} (C_L^{3/2}/C_D)} \sqrt{\frac{2W/S}{\rho}} \quad (31)$$

The mass of the electric battery does not change during the flight phases. The total battery mass fraction is calculated as the sum of fractions for different mission segments.

$$MF_{batt} = \sum_{i=1}^{n_{seg}} MF_{batt}^{i} \quad (32)$$

2.1.6. Post-processing

The total mass of an aircraft is the key parameter for estimation of the whole aircraft configuration. At this design stage, many parameters are defined as the ratio to total mass. Parameters like the wing area, wing span, forward flight motor power, and VTOL propeller area are calculated at this stage. These parameters are then used to create the carpet plots or run the numerical optimization.

2.2. Design evaluation

Integrated analysis evaluates the characteristics of an aircraft for a given set of design requirements, assumptions, and design parameters. Design evaluation is used to determine the best possible combination of wing and power loadings. There are two possible approaches: graphical (sizing matrix plot) and numerical (optimization). Both are widely used at the sizing stage.

2.2.1. Sizing matrix plot

A sizing matrix plot is a useful method of visualizing the design space and manually selecting the aircraft configuration to be developed. W/S and P/W are varied within the bounds selected by the designer. The appropriate bounds for W/S are about 10 to 110% of $(W/S)_{stall}^{FW}$, the maximum wing loading satisfying the stall speed requirement in FW mode. Appropriate values for the P/W bounds for propeller-driven aircraft are within the range of 2–30 W/N. A typical value of P/W for this type of aircraft is 6–10, and thus bounds of 2–20 will provide better visualization of the design space. Each combination of W/S and P/W will produce an aircraft with different mass, geometry, and propulsion properties. The contours of the most important and representative parameters are then plotted. Parameters to be plotted include several mass quantities, such as the total mass and battery mass, and geometries such as the wing span and VTOL propeller diameter. Performance constraint curves should be plotted as well. An example of a total mass contour plot for an aircraft with 2 kg of payload, 5 minutes of hovering, 1 hour of cruise endurance, and a maximum speed of 90 km/h is shown in Fig. 7. Aircraft total mass is increasing in direction of higher power and wing loading. Battery mass fraction is directly proportional to $\sqrt{W/S}$ as can be seen from equation (31). Larger required capacity of the batteries forces total mass increase. Higher power loading requires more powerful and heavier motors.

Fixed wing aircraft sizing theory [10] suggests that the extremum points of constraint curves be used as an optimum configuration. There are two extremum points in Fig. 7: the intersection of cruise speed with the rate of climb, which corresponds to the minimum power loading, and the intersection of the stall speed with the rate of climb curve, which corresponds to the maximum wing loading condition. The first point is more valuable in terms of the most parameters. The aircraft at this point has a lower total mass and battery mass and a slightly smaller diameter of VTOL propeller. The wing span is quite an important parameter for a small UAV not only in terms of performance but also in terms of

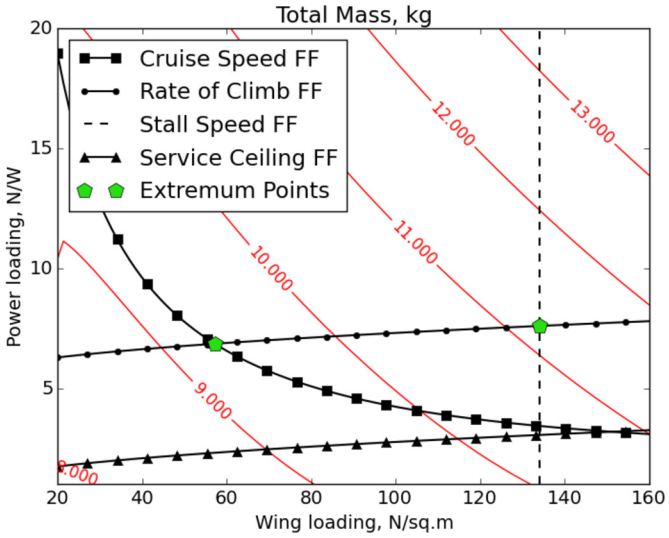

Fig. 7. Sizing matrix plot of aircraft total mass.

Table 5
Example optimization formulation.

	Variable		Value
Minimize:	Total mass		
Subject to:	Maximum speed	$\geq$	90 km/h
	Rate of climb in FW mode	$\geq$	3 m/s
	Rate of climb in VTOL mode	$\geq$	3 m/s
	Stall speed	$\leq$	45 km/h
	Service ceiling	$\geq$	1000 m
	Mass of the battery	$\leq$	2.5 kg
	Wing span	$\leq$	3.0 m
	VTOL propeller diameter	$\leq$	20 in

storage and transportation. In this particular example, the wing span is 3.74 and 2.69 m for the first and second points respectively. The difference of 1.05 m or 39% of the wing span may be critical. Thus, the heavier but more compact configuration can also be chosen as the initial design. Overlaying different contours in one figure will make the designer's selection easier. After choosing the combination of wing and power loadings, the designer should run the integrated analysis again to obtain full information about the aircraft configuration at the selected design point.

2.2.2. Optimization

While a sizing matrix plot is a useful tool for visualization and manual selection of a design point, numerical optimization is a useful tool to find a design point that strictly satisfies certain requirements. Optimization algorithms may be used in addition to sizing matrix plots as well as independently, for example as part of a design framework. The analysis methods described in this paper are analytic equations that are represented as smooth functions. Thus, gradient-based optimization methods are the most suitable choice for these types of problems. The SLSQP algorithm of Python's SciPy [22] numerical library is used in this research; however any other constrained optimization algorithm would work.

The design variables for the optimization problem are similar to that of the sizing matrix plot, namely the wing loading and power loading. Table 5 shows an example of an optimization formulation with a single objective and seven constraint functions.

The results of numerical optimization using the same set of requirements as discussed in the previous subsection are a wing loading of 77.26 N/m^2 and power loading of 7.20 N/W. There are three active constraints in this case: the rate of climb in forward flight mode, the propeller diameter, and the wing span. It can be observed that the optimum point in this particular case is different from extremum points of the sizing matrix plot. The solution is constrained by geometrical parameters in this formulation. Numerical optimization provides more accurate and flexible tool while sizing matrix plot helps to understand the general trends.

2.3. Tail sizing and VTOL propulsion arrangement

FW-VTOL UAV has more geometrical and other constraints comparing to conventional FW UAV. It narrows the freedom of tail configuration selection and its sizing. The most of UAVs have a pusher propeller configuration to allow a wider field of view for sensors and cameras located in frontal part of the fuselage. Inverse V-tail or twin boom T-tail (also called Π-tail) configurations are common for UAVs with pusher propeller. Upper position of horizontal tail reduces the propeller slipstream effect on a tail. Multicopter type control is very sensitive to changes in moments of inertia (MOI), especially in yawing. Length of an aircraft should be minimized to reduce the MOI around z-axis. Wing, tail, and propellers are arranged to minimize the overall dimensions of aircraft while leaving space for normal operation and adjustment of propellers.

This subsection describes sizing of a twin boom T-tail configuration. V-tails can be sized using a similar approach. A number of geometrical problems should be solved to arrange the FW and VTOL propellers, wing, and tail. Fig. 8 shows the general arrangement of FW-VTOL UAV elements. The aircraft CG should be located as close as possible to the CG of VTOL propeller-motor system. This arrangement minimizes power required to trim the aircraft and simplify the control in multicopter mode. In addition, the clearance between propellers and all the structural elements should be provided for safety, uniform thrust through the propeller disc, and adjustment at later design stages.

The span of the horizontal tail (HT) is estimated as the sum of VTOL and FW propeller diameters. It provides enough clearance for both propellers as can be seen on Fig. 8.

$$b_{HT} = D_{prop}^{VTOL} + D_{prop}^{FW} \tag{33}$$

Clearance between propeller and airframe c_{prop} is provided for safety reasons as well as for eliminating blockage of tip vortex, which may lead to non-symmetric thrust through the propeller disc. The most aft location of the front propellers and the most forward location of the rear VTOL propellers are determined from wing planform shape, propeller clearance, and propeller diameter parameters. The most aft location of the front propeller is calculated as:

$$x_{PF} = x_w + \frac{b_{HT}}{2}\tan\Lambda_{LE_w} - \frac{D_{prop}^{VTOL}/2 - c_{prop}}{\cos\Lambda_{LE_w}} \tag{34}$$

The most forward location of the rear propeller as:

$$x_{PR} = x_w + c_{r_w} + \frac{b_{HT}}{2}\tan\Lambda_{TE_w} + \frac{D_{prop}^{VTOL}/2 + c_{prop}}{\cos\Lambda_{TE_w}} \tag{35}$$

Aircraft CG is located at CG of VTOL propeller-motor system. Location of propellers can be slightly adjusted at detailed design stage when exact CG of the structure and subsystems is known.

$$x_{CG} = \frac{1}{2}(x_{PR} - x_{PF}) \tag{36}$$

The leading edge of vertical tail (VT) in the most compact configuration is located at clearance distance from rear propeller disc.

$$x_{VT} = x_{PR} + D_{prop}^{VTOL}/2 + c_{prop} \tag{37}$$

Tail volume coefficient method is implemented to size horizontal tail and vertical tail [9,13,23]. The volume coefficient defines ratio between tail force and wing geometry. This method is widely

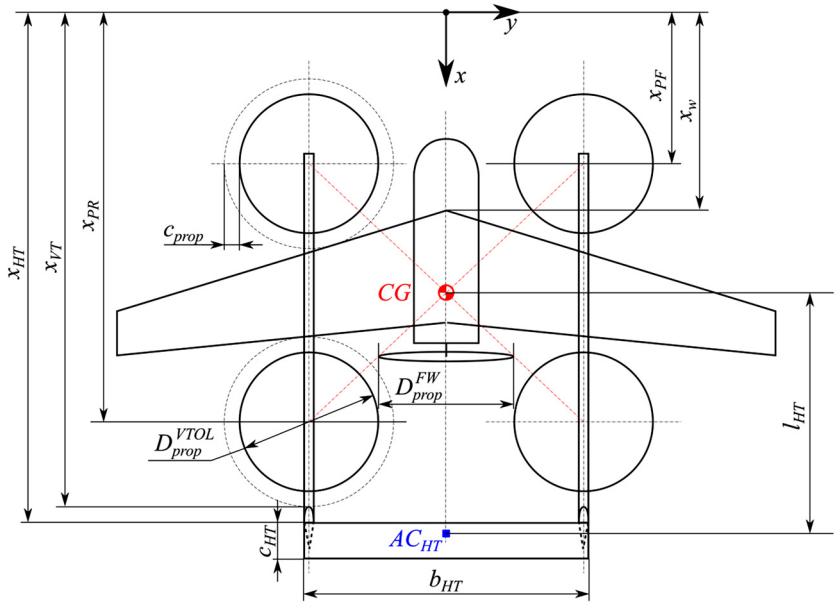

Fig. 8. FW-VTOL aircraft layout.

used at early conceptual design stages. Nicolai defines the HT volume coefficient as [23]:

$$C_{HT} = \frac{l_{HT} S_{HT}}{\bar{c}_w S_w} \tag{38}$$

where l_{HT} the distance from CG to aerodynamic center of HT. Aerodynamic center is located at approximately 25% of mean aerodynamic chord (MAC). Vertical tail volume coefficient is calculated in a similar way.

$$C_{VT} = \frac{l_{VT} S_{VT}}{b_w S_w} \tag{39}$$

There is no recommendation for volume coefficients of this particular type of aircraft. The values of aircraft flying at similar flight conditions can be used, 0.53–0.70 for C_{HT}, and 0.022–0.032 for C_{VT} [23]. The assumed range covers sailplane, intelligence, surveillance and reconnaissance (ISR), and single propeller general aviation aircraft. Tip chord of VT is equal to chord of HT in this configuration. Tail area and other geometry properties are determined by implementing fixed-point iteration loop described below. Initial assumption for tail moment arms is:

$$l_{HT} = l_{VT} = x_{vt} - x_{CG} \tag{40}$$

HT area and chord can be determined from the volume coefficient equation.

$$S_{HT} = \frac{C_{HT} \bar{c}_w S_w}{l_{HT}} \tag{41}$$

$$c_{HT} = S_{HT} / b_{HT} \tag{42}$$

Area of the VT is calculated similarly

$$S_{VT} = \frac{C_{VT} b_w S_w}{2 l_{VT}} \tag{43}$$

Note that in twin boom configuration the area of VT is divided by two. The span of the tapered VT is calculated as follows.

$$b = \frac{2 S_{VT}}{c_{HT}(1/\eta_{VT} + 1)} \tag{44}$$

Here η_{VT} is the taper ratio of the vertical tail. Leading edge sweep and taper ratio of a VT should be provided by designer based on previous experience or other considerations. When the geometry of HT and VT are known, the length of moment arms can be updated.

$$l_{HT} = (x_{VT} + b_{VT} \tan \Lambda_{LE_{VT}} + 0.25 c_{HT}) - x_{CG} \tag{45}$$

$$l_{VT} = (x_{MAC_{VT}} + 0.25 \bar{c}_{VT}) \tag{46}$$

MAC for a single tapered wing configuration is calculated from the given geometrical equation.

$$x_{MAC} = x_{CG} + \frac{S_{VT}(c_{r_{VT}} + 2c_{t_{VT}})}{3(c_{r_{VT}} + c_{t_{VT}})} \tag{47}$$

$$\bar{c}_{VT} = c_{r_{VT}} - \frac{2(c_{r_{VT}} - c_{t_{VT}})(0.5 c_{r_{VT}} + c_{t_{VT}})}{3(c_{r_{VT}} + c_{t_{VT}})} \tag{48}$$

Calculation of HT and VT area should be repeated until tail area convergence. Solution typically converges within 3–5 iterations.

2.4. Resizing

Initial sizing generates the first guess of the aircraft mass, geometry, and parameters of the required propulsion system. The exact model of the propulsion system components is selected based on the required power, thrust, and battery capacity. In many cases, the gear manufacturer provides a recommendation about the best-matching parts, such as the motor, propeller, and electric controller. The total mass of the aircraft should be updated using the following equation:

$$M_{TO} = \frac{M_{propulsion}^{VTOL} + M_{propulsion}^{FW} + M_{payload} + M_{batt}}{1 - (MF_{struct} + MF_{subsyst} + MF_{avion})} \tag{49}$$

At this stage, the mass of the propulsion system, payload, and battery are known. The mass fractions of the structure, subsystem, and avionics come from assumed values as explained in subsection 2.1.2. If all components are selected properly, the variation of total mass will be within 10–15% of the result of the initial sizing. The battery capacity required to complete the mission profile should be calculated next. The same methodology as explained in Subsection 5 of the Integrated Analysis section is used with updated values of E_{spec}, M_{TO}, and DL. Several parameters of the resized aircraft should be checked in order to guarantee that the

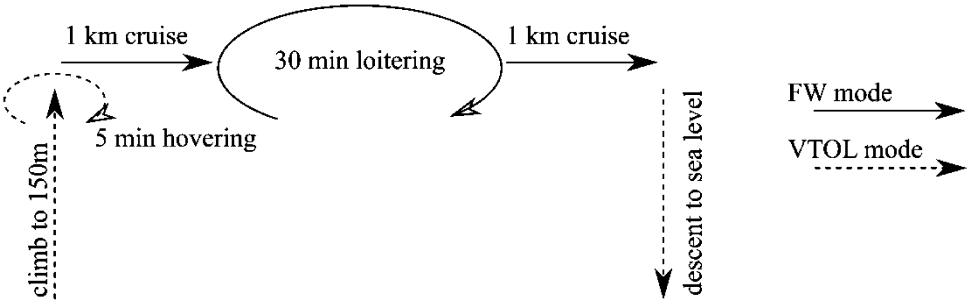

Fig. 9. Mission profile.

Table 6
3.5 kg VTOL-FW electric UAV design requirements.

Parameter	Value	Remarks
Payload mass	0.3 kg	
Rate of climb in VTOL mode	3.0 m/s	
Rate of climb in FW mode	3.0 m/s	
Maximum cruise speed	30 m/s	
Stall speed in FW mode	11.1 m/s	40 km/h
Cruise altitude	150 m	FAA requirement below 400 ft.
Structure mass fraction	40%	Airframe, retractable landing gear
Avionics mass fraction	5%	On-board computer, radio receiver/transmitter
Subsystem mass fraction	15%	Servo, FPV camera
Propeller gap	0.05 m	Gap between VTOL propeller and structure
HT volume coefficient	0.55	
VT volume coefficient	0.028	

design requirements are satisfied. The thrust-to-weight ratio generated at the initial sizing stage should be compared with the exact value. The value of the battery capacity should be compared with the required value. The new components should be selected if the current set does not match the required values.

3. Case study

The methodology proposed in this research is implemented to design a 3.5-kg VTOL-FW electric UAV. The current aircraft is a test prototype of a larger 25-kg UAV that is currently under development. Table 6 shows the design requirements.

Part 107 (UAV) of the FAA regulations states that commercial and governmental UAVs should operate at altitudes below 400 ft (120 m). A cruising altitude of 150 m is assumed to provide some margin for performance and mission battery calculations. The structural mass fraction is assumed to be 40% of the total mass. It includes the airframe and retractable landing gear. The on-board computer (avionics) mass fraction is assumed to be 5% of the total mass. The subsystem includes all servos for control surfaces and an FPV camera. The mass fraction of the subsystem is assumed to be level of 15%. The aircraft should be able to hover at a power setting of 50% or lower. Fig. 9 shows the mission profile. A simple mission profile is assumed with VTOL, climbing to cruise altitude at 3 m/s, 5 minutes of hovering, cruising for a total of 2 km, 30 minutes of loitering, and descent to sea level. It is assumed that the battery capacity required for transition from VTOL to FW flight is included in the 5 minutes of hovering.

Fig. 10 shows the sizing matrix plot for the given set of aircraft design requirements. The figure shows that the required contour of a target mass of 3.5 kg is close to the extremum point. It is decided to develop the design with the minimum wing span. Performance constraint curves show that there is still a power loading margin for the cruise speed. The actual cruise speed is greater than the required value of 30 m/s. The service ceiling constraint is not active for this type of aircraft and may be skipped in future designs of UAVs cruising near to sea level.

Table 7
Comparison of initial sizing, resizing, and actual aircraft built.

Parameter	Unit	Initial sizing	Resizing	Actual UAV	Resizing Error, %
Wing loading	N/m^2	105.9	105.9	110.3	−3.9
Power loading	W/N	9.178	7.576	7.936	−4.5
VTOL thrust-to-weight ratio	–	2.000	1.863	1.952	−4.6
Wing span	m	1.705	1.775	1.700	+4.4
Wing area	m^2	0.330	0.358	0.328	+9.1
Total mass	kg	3.568	3.865	3.688	+4.8
Structure mass	kg	1.427	1.546	1.410	+9.6
Battery capacity	mAh	4993	5792	5100	+13.6
Horizontal tail area	m^2	0.0571	0.0613	0.0608	+0.8
Vertical tail area	m^2	0.0089	0.0100	0.0096	+4.2
VTOL propulsion mass	kg	0.414	0.535	0.535	N/A
FF propulsion mass	kg	0.145	0.129	0.129	N/A
VTOL maximum thrust	kg	7.134	7.200	7.200	N/A
VTOL propeller diameter	in	14.13	13.00	13.00	N/A
FF motor power	W	321.1	287.1	287.1	N/A
FF propeller diameter	in	16.50	11.00	11.00	N/A

Table 7 shows the comparison of calculated data and the actual manufactured FW-VTOL electric UAV data. The initial sizing column represents the selected design point shown in Fig. 10.

The total mass of the initially sized aircraft is 3.57 kg, which is 2% higher than the target mass. Electric motors, propellers, and batteries are selected based on the results of initial sizing. It is decided to move towards ease of maintainability of the aircraft, and thus the same models of motors are selected for use with VTOL and FW propulsions. The propulsion system is composed of five T-motor U3 motors. Initial sizing calculations suggest the use of a 14.13-inch propeller for VTOL and a 16.50-inch one for FW. Based on the manufacturer's compatibility table, the 13-inch propeller is selected for VTOL and the 11-inch one for FW propulsion. The motor with the 13-inch propeller generates 1.8 kg of thrust, 0.9% more than calculated in the initial sizing. The motor with the 11-inch propeller is able to generate 287 W of power in FW mode, 10% less than the result of the initial sizing. This selection causes a slightly lower rate of climb in FW mode and will not affect any other performance constraints. The resizing column in Table 7 demonstrates the calculated parameters of the resized aircraft with the new propulsion system and battery. Fig. 11 shows the error between resized and the actual aircraft.

The mass of the propulsion and battery is slightly higher than that calculated at the initial sizing stage. As a result, the total mass of the resized aircraft is increased to 3.87 kg. The target mass is exceeded by 10%. The initially assumed specific energy of the battery of 150 Wh/kg was too optimistic. The actual energy density of the selected 5100-mAh battery is 130 Wh/kg. The required battery capacity of the resized aircraft exceeds that of the actual battery by 13.6%. The last column of Table 7 shows the parameters of the ac-

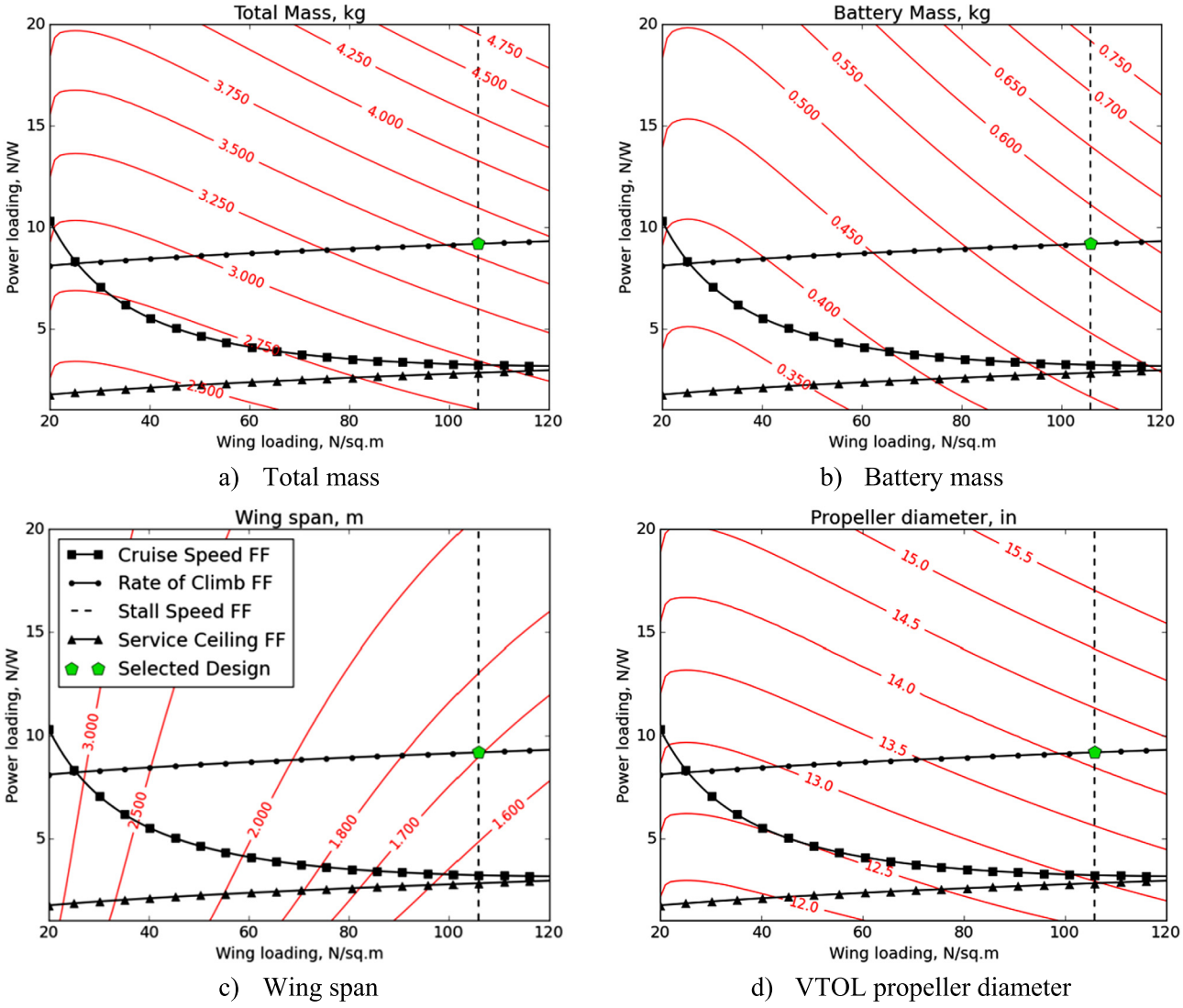

Fig. 10. Sizing matrix plot of several mass and configuration parameters.

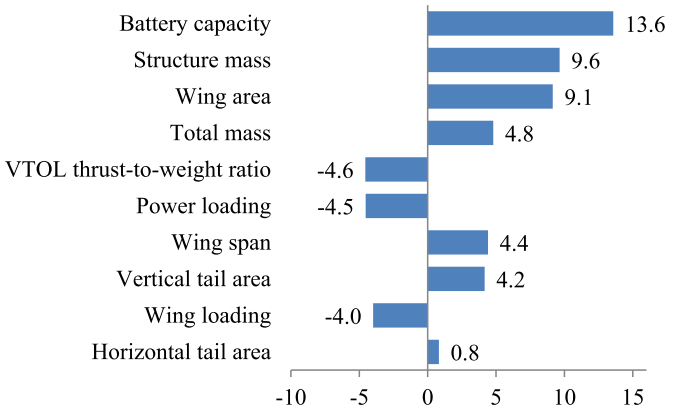

Fig. 11. Resizing error.

tual aircraft built. The mass of the actual aircraft is 3.688 kg, 177 g less than the value calculated at the resizing stage. The area of HT and VT was predicted with accuracy of 0.8 and 4.2% respectively. The minor mass reduction was achieved by optimizing the airframe structure with the mass fraction of 38% of total mass versus the assumed value of 40%.

As seen from the last column of Table 7, the prediction error of the FW-VTOL electric UAV sizing process is within the 10% threshold. This level of error is acceptable at early design stages.

4. Conclusions

This research presents a novel methodology for sizing of FW-VTOL electric UAVs. The overall sizing process is composed of two major parts. The initial sizing converts the design requirements into basic parameters of a future aircraft. The actual components of the propulsion system and battery are selected based on the results of initial sizing. Aircraft resizing is performed in the next stage. Resizing updates the parameters of the aircraft using information about selected parts. The core of the initial sizing is the integrated analysis. FW constraints analysis, electric propulsion sizing, mission battery calculation, total mass calculation, and geometry analysis methods are combined into the FW-VTOL electric UAV integrated analysis. Two methods are proposed to determine the candidate configuration for future development: graphical (sizing matrix plot) and numerical (optimization). Both methods may be used together or separately.

A real 3.5-kg FW-VTOL electric UAV design case study is presented. The aircraft is designed to operate at speeds of up to 30 m/s with a mission profile that includes hover, cruise, and loiter

phases. The results of the initial sizing and resizing are compared with the parameters of an aircraft that was actually built. The developed sizing process predicts the parameters of the aircraft with accuracy of within 10% for most of the parameters. The developed sizing methodology provides a useful tool for aircraft designers at early design stages.

Conflict of interest statement

No conflicts.

Acknowledgements

This research was supported by Konkuk University Brain Pool 2017, Korea Institute for Advancement of Technology (Grant number: R0004086), and National Research Foundation of Korea (Grant number: 2016K1A3A1A12953685).

References

[1] UAV factory – unmanned platforms and subsystems [Online]. Available: http://www.uavfactory.com/product/69. (Accessed 18 October 2016).
[2] G. Girishkumar, B. McCloskey, A.C. Luntz, S. Swanson, W. Wilcke, Lithium–air battery: promise and challenges, J. Phys. Chem. Lett. 1 (14) (Jul. 2010) 2193–2203.
[3] M. Hepperle, Electric flight – potential and limitations, presented at the AVT-209 Workshop on Energy Efficient Aircraft Configurations, Technologies and Concepts of Operation, Sao José dos Campos, 2013.
[4] Y. Li, J. Yang, J. Song, Design principles and energy system scale analysis technologies of new lithium-ion and aluminum-ion batteries for sustainable energy electric vehicles, Renew. Sustain. Energy Rev. 71 (May 2017) 645–651.
[5] S. Stückl, J. van Toor, H. Lobentanzer, VOLTAIR – the all electric propulsion concept platform – a vision for atmospheric friendly flight, in: 28th International Congress of the Aeronautical Sciences, ICAS, 2012.
[6] C.A. Luongo, et al., Next generation more-electric aircraft: a potential application for HTS superconductors, IEEE Trans. Appl. Supercond. 19 (3) (Jun. 2009) 1055–1068.
[7] Rekord-Motor SP260D und Extra 330LE, Siemens AG (in German).
[8] G.M. Hoffmann, H. Huang, S.L. Waslander, C.J. Tomlin, Quadrotor helicopter flight dynamics and control: theory and experiment, in: Proc. of the AIAA Guidance, Navigation, and Control Conference, vol. 2, 2007, p. 4.
[9] D.P. Raymer, Aircraft Design: A Conceptual Approach, 5th edition, AIAA, Reston, VA, 2012.
[10] S. Gudmundsson, General Aviation Aircraft Design: Applied Methods and Procedures, 1st edition, Butterworth–Heinemann, Oxford, Waltham, MA, 2013.
[11] L.K. Loftin, Subsonic Aircraft: Evolution and the Matching of Size to Performance, NASA, RP1060.
[12] J. Roskam, Rapid sizing methods for airplanes, presented at the Aircraft Design Systems and Operations Meeting, Colorado Springs, CO, USA, 1985.
[13] J. Gundlach, Designing Unmanned Aircraft Systems: A Comprehensive Approach, Amer. Inst. of Aeronautics, Reston, VA, 2011.
[14] C.E.D. Riboldi, F. Gualdoni, An integrated approach to the preliminary weight sizing of small electric aircraft, Aerosp. Sci. Technol. 58 (2016) 134–149.
[15] J.D. Keith, D.W. Hall, Rapid sizing methodologies for VTOL UAVs, in: 47th AIAA Aerospace Sciences Meeting including The New Horizons Forum and Aerospace Exposition, 2009, p. 1617.
[16] D.P. Paine, J.D. Kiser, Aerial Photography and Image Interpretation, 3rd ed., Wiley, Hoboken, 2012.
[17] Aye Aye Maw, T. Maxim, N. Le Viet Thang, L. Jae-Woo, UAV mapping mission design based on operation specific requirements, presented at the Korean Society for Aeronautical and Space Sciences Spring Conference Gangwon-do, Korea, 2016.
[18] eCalc – the most reliable RC Calculators on the Web for electric motors [Online]. Available: http://ecalc.ch/calcinclude/help/xcoptercalchelp.htm. (Accessed 31 August 2016).
[19] J.G. Leishman, Principles of Helicopter Aerodynamics, Cambridge University Press, 2002.
[20] T-MOTOR [Online]. Available: http://www.rctigermotor.com/. (Accessed 27 October 2016).
[21] J. Roskam, C.T. Lan, Airplane Aerodynamics and Performance, revised edition, DARcorporation, Lawrence, Kan, 2016.
[22] Optimization (scipy.optimize) — SciPy v0.18.1 reference guide [Online]. Available: http://docs.scipy.org/doc/scipy/reference/tutorial/optimize.html. (Accessed 04 October 2016).
[23] L. Nicolai, G. Carichner, Fundamentals of Aircraft and Airship Design, Amer. Instit. of Aeronautics and Astronautics, Reston, VA, 2010.